Photodiagnosis and Photodynamic Therapy 13 (2016) 81–90

Contents lists available at ScienceDirect

Photodiagnosis and Photodynamic Therapy

journal homepage: www.elsevier.com/locate/pdpdt

# Protoporphyrin IX-loaded magnetoliposomes as a potential drug delivery system for photodynamic therapy: Fabrication, characterization and in vitro study

Harun Basoglu[a,*], Mehmet Dincer Bilgin[b,1], Mustafa Muammer Demir[c,2]

[a] Department of Biophysics, Medical Faculty, Bezmialem Vakif University, Fatih, Istanbul 34093, Turkey
[b] Department of Biophysics, Medical Faculty, Adnan Menderes University, Aydin, Turkey
[c] Department of Materials Science and Engineering, Faculty of Engineering, Izmir Institute of Technology, Izmir, Turkey

ARTICLE INFO

*Article history:*
Received 30 July 2015
Received in revised form 9 December 2015
Accepted 28 December 2015
Available online 2 January 2016

*Keywords:*
Protoporphyrin IX
Magnetoliposomes
Iron oxide nanoparticles
Photodynamic therapy
MCF-7 cells

ABSTRACT

*Background:* Protoporphyrin IX (PpIX) is a well-known photosensitizer that has great potential for use in photodynamic therapy (PDT). However, aggregation behavior of PpIX in neutral water makes it inappropriate for physiological studies. PpIX-loaded magnetoliposomes (MLs) were fabricated to increase PpIX biocompatibility. PpIX-loaded ML physical properties were characterized, and PpIX-loaded ML drug release behavior was investigated under the influence of an external magnetic field and heat. Toxicity and photodynamic effects of the complex were also examined using in vitro experiments with MCF-7 human breast cancer cells.
*Methods:* The magnetoliposomes were prepared with DPPC, DSPE-PEG2000 lipids and $Fe_3O_4$ nanoparticles. The toxicity and in vitro photodynamic effects of the PpIX-loaded MLs at various concentrations were studied using the MCF-7 cell line.
*Results:* The produced PpIX-loaded MLs exhibited an average hydrodynamic diameter of 221 nm; however, TEM measurements indicated that the diameter of the PpIX-loaded MLs varied between 166 and 720 nm. The iron content of the MLs affected cell viability less than the content of the iron free liposomes. Cell viability was reduced to 66% when the concentration of the PpIX-loaded MLs was 350 nM, but when white light was applied for 5 min, all of the cells that were exposed to concentrations of 250 nM and higher PpIX died within 24 h.
*Conclusion:* The results of this study demonstrated the effective application of PpIX-loaded MLs for in vitro photodynamic therapy at nanomolar concentrations. The results also indicated that an LED light source provided sufficient energy to stimulate the PpIX molecules.



## 1. Introduction

Magnetoliposomes (MLs) consist of liposomes and magnetic nanoparticles. MLs have high potential for the delivery of various bioactive molecules that could be used for therapeutic applications in both humans and animals [1,2]. Magnetic nanoparticles contribute multifunctional properties to MLs. For instance, MLs can be used as an image contrast agent, they can provide hyperthermic cancer treatment by heating nanoparticles in an alternating current electromagnetic field, and they can be used for liposomal drug delivery and thermosensitive drug release [3–5]. Diverse lipids, nanoparticles and drug combinations have been studied in the literature, and efficient incorporation of drugs into MLs has been shown to depend on the selection of lipids and nanoparticles, as well as on drug interactions [6–8].

Photodynamic therapy (PDT) uses photosensitizers and visible light to treat various types of cancer, such as lung, esophageal, gastric, cervical and bladder cancer. It is also used to treat non-malignant diseases, such as atherosclerosis, psoriasis, and age-related macular degeneration [9,10]. Alone, photosensitizers and light are harmless, but cell damage results when they are combined in the presence of adequate molecular oxygen in tissue [11,12]. When a photosensitizer is irradiated by an appropriate light wavelength, the photosensitizer is promoted from the ground state ($S_0$) to the first excited singlet state ($S_1$), and then it passes to the longer-

* Corresponding author. Fax: +90 2124531883.
*E-mail addresses:* hbasoglu@bezmialem.edu.tr (H. Basoglu), mdbilgin@gmail.com (M.D. Bilgin), mdemir@iyte.edu.tr (M.M. Demir).
[1] Fax: +90 2562123169.
[2] Fax: +90 2327507509.

http://dx.doi.org/10.1016/j.pdpdt.2015.12.010
1572-1000/

lived triplet state ($T_1$) by an intersystem crossing pathway. The excited photosensitizer returns to ground state from triplet state and either emits light called fluorescence or undergoes a radiationless transition, whereby energy is absorbed by or transferred to another particle or system [13]. In this process, the photosensitizer acts as an energy transducer and transfers energy to molecular oxygen, resulting in the production of many reactive oxygen species (ROS), such as singlet oxygen ($^1O_2$), hydrogen peroxide($H_2O_2$), and superoxide radicals ($O_{2-}$). Singlet oxygen ($^1O_2$) is a predominant cytotoxic agent in PDT [14–16].

PDT is a clinically approved, minimally invasive therapeutic procedure. However, cancer patients may have medications remaining in their bodies for up to six weeks after administration, and their quality of life can be severely affected by PDT side effects. The most common side effects are mild to moderate burning, stinging, erythema and pain [17]. New drug research is continuing around the world to minimize these types of side effects and increase the use and efficacy of PDT [18].

Protoporphyrin IX (PpIX) is a metal-free porphyrin that is a precursor of heme. The biosynthesis of porphyrin starts with the synthesis of 5-aminolevulinic acid (5-ALA) [19,20]. PpIX exists as a monomer in the pH range 0–3, as an aggregate in the pH range 3–8 and as a dimer in any pH greater than 8 [21]. Aggregation behavior of PpIX in neutral water makes it inappropriate for use in physiological studies. However, indirect application of PpIX is made possible by mediation with 5-ALA, which is a method that has been used for bladder cancer [22]. PpIX concentrations correlate with cellular 5-ALA concentration levels; therefore, concentrations of 5-ALA at the mM level have been examined in cell cultures [22,23].

We hypothesize that the usage of PpIX-loaded MLs in a cell line with PpIX concentrations lower than the concentration of 5-ALA-mediated PDT reported in literature can result in efficient therapeutic effects at nanomolar concentrations. Moreover, PpIX-loaded MLs can be used to for magnetic hyperthermia and for magnetic targeting because of the incorporated magnetic nanoparticles. The first aim of this study was first to fabricate PpIX-loaded MLs and characterize their structure. For structure characterization, we performed size and zeta potential measurements to understand ML hydrodynamic diameters and stability. We also examined magnetic hyperthermia over a series of temperature increments under an AC magnetic field. Turbidity testing was performed to assess magnetic targeting properties. The second aim of this study was to examine toxicity and photodynamic effects of PpIX-loaded MLs on the MCF-7 human breast cancer cell line, which represents one of the most aggressive forms of cancer.

## 2. Materials and methods

Phospholipids 1,2-dihexadecanoyl-*sn*-glycero-3-phosphocholine (DPPC), 1,2-dipalmitoyl-*sn*-glycero-3-phosphoethanolamine-*N*-[methoxy(polyethylene glycol)-2000] (ammonium salt) (DSPE-PEG2000) and an extruder set with 200-nm PC membranes were purchased from Avanti Polar Lipids (Alabaster, AL, USA). $Fe_3O_4$ nanoparticles with an average size of 10 nm in $H_2O$ and all other chemicals (including protoporphyrin IX), which were analytical grade and used without further purification, were purchased from Sigma–Aldrich (Sigma Chemical Company, Saint Louis, MO, USA).

### 2.1. Preparation of PpIX stock solution

Stock solution was prepared by dissolving 1 mg PpIX in 5 ml of a chloroform–methanol mixture (2:1 (v/v)) and mixing well by vortexing. The stock solution was kept at +4 °C after sealing the top of the container with parafilm. The stock solution was used within 5 days.

### 2.2. Preparation of PpIX-loaded magnetoliposomes

DPPC and DSPE-PEG2000 (99%:1% (w/w)) were dissolved in a mixture of chloroform and methanol (2:1 (v/v)) in a round-bottom flask. Different concentrations of PpIX (20 μM, 40 μM and 60 μM) were added to the phospholipid mixture and dried in a rotary evaporator (Heildolph Instrument, Schwabach, Germany) under reduced pressure at 50 °C to form a thin film on the inner surface of the flask. The thin film was hydrated by adding PBS while being rotated at 120 rpm at atmospheric pressure in a 60 °C water bath for 10 min. Then, the mixture was sonicated (Elmasonic E 100H, Singen, Germany) at 55–60 °C for 10 min. The resulting preparation was extruded 15 times through 200-nm polycarbonate membranes using the Avanti extruder set, and the PpIX-loaded liposomes were produced. Subsequently, different amounts of $Fe_3O_4$ nanoparticles (0.175, 0.35 and 0.5 mg $Fe_3O_4$) were prepared by mixing 1 mlPBS 60 °C in an Eppendorf tube and adding PpIX-loaded liposomes. The mixture was sonicated for 15 min to obtain the PpIX-loaded magnetoliposomes (MLs). The PpIX-loaded MLs were dialyzed overnight using 20 K Slide-A-Lyzer Dialysis Cassettes (Thermo Scientific, IL, USA) to remove unencapsulated PpIX and nanoparticles. Dialyzed and non-dialyzed samples were prepared to calculate encapsulation efficiency. Details can be found in the "Evaluation of PpIX Encapsulation and Release from Thermosensitive Magnetoliposomes" section of this manuscript.

### 2.3. Magnetoliposome preparation

The magnetoliposome preparation procedure is similar to that of the PpIX-loaded MLs. The difference is that PpIX solution was not added to the phospholipid mixture, but 0.5 mg $Fe_3O_4$ nanoparticles were added to obtain the MLs. The number of nanoparticles for ML preparation was chosen considering the zeta potentials of PpIX-loaded MLs experiment.

### 2.4. Liposome preparation

Liposomes were prepared using a procedure similar to that used for ML preparation, except the liposomes did not include $Fe_3O_4$ nanoparticles.

### 2.5. Size and zeta potential determination

The zeta potentials and hydrodynamic diameters of the samples, including the mean and polydispersity of the samples, were determined by dynamic light scattering at 25 °C via Zetasizer Nano ZS (Malvern, UK).

### 2.6. Transmission electron microscopy

PpIX-loaded MLs and MLs were observed by transmission electron microscopy (TEM) using an FEI Tecnai G2Spirit BioTwin (Hillsboro, OR, USA) operating at 80 kV. The samples were prepared by casting a drop of ML dispersion onto a 200 mesh copper grid coated with carbon film and allowing it to air-dry before placing it into the microscope.

### 2.7. Evaluation of PpIX encapsulation and release from thermosensitive magnetoliposomes

The PpIX encapsulation and release assay was based on the detection of dialyzed and non-dialyzed PpIX-loaded ML fluorescence; the procedure was modified from one previously published

by Pradhan et al. [3]. Dialyzed and non-dialyzed PpIX-loaded ML concentrations were used to calculate encapsulation instead of the initial PpIX concentration because initial PpIX was dissolved in chloroform and methanol, while PpIX-loaded MLs were in water, meaning a comparison may not yield reliable results. Encapsulation efficiency, percentage of PpIX release and the percentage of fluorescence emission were calculated (Supplementary material).

### 2.8. Measurement of Fe in PpIX-loaded MLs

Inductively Coupled Plasma-Mass Spectrometer (ICP-MS) was used to investigate the amount of encapsulated $Fe_3O_4$ nanoparticles by measuring the Fe content of the PpIX-loaded MLs. For this purpose, 6 ml $HNO_3$ and 2 ml $H_2O_2$ were added to samples and the temperature was increased to 175 °C over 15 min using a digestion microwave system (CEM, Mars5, NC, USA), and the mixture was held for another 15 min at that temperature for digestion. After that, samples were diluted, and Fe content was measured using ICP-MS (Agilent 7500ce, CA, USA). Dialyzed and non-dialyzed PpIX-loaded MLs having different amounts of $Fe_3O_4$ nanoparticles were compared to assess encapsulated iron content percentage.

### 2.9. Measurement of PpIX-loaded ML heating ability under an electromagnetic field

Assessment of PpIX-loaded ML heating ability was performed under an $8.947 \pm 2\%$ μT, 50 Hz AC magnetic field generated by a solenoid. Magnetic field was measured by an Emdex II (CA, USA), and temperature changes were measured by a Fluke 568 infrared thermometer (WA, USA) with a wire probe. PpIX-loaded MLs were transferred to Eppendorf tubes and placed in the solenoid. An equal amount of water was also placed in the solenoid as a control for the heat generated by the solenoid. Temperature changes of the PpIX-loaded MLs and water were determined by measuring temperatures at 30 and 60 min under the electromagnetic field. Real temperature changes were obtained by subtracting the temperature of water from the temperature of the PpIX-loaded MLs.

### 2.10. Turbidity measurement

Sedimentation stability and magnetic responses were determined by turbidity measurements in optical cuvettes using a spectrophotometer as previously described [24]. In brief, $Fe_3O_4$ nanoparticles were diluted with ultrapure Milli-Q water and placed in glass cuvettes; every 5 s up to 45 min, spectrophotometric measurements were collected at a wavelength of 650 nm and were denoted as $A^{\circ}_{650}$. $Fe_3O_4$ concentrations for both naked nanoparticles and PpIX-loaded MLs were same. Then, NE1816 permanent magnets (IBSmagnet, Berlin, Germany) were positioned symmetrically on the right and left side of the cuvette holder. Four magnets, with an average magnetic field property of 4 T/m, were used on each side, and spectrophotometric measurements were performed as described above; these were defined as $A_{650}$. The same measurements were repeated for the PpIX-loaded MLs. A graph illustrating time versus $A_{650}/A^{\circ}_{650}$ was prepared to identify sedimentation stability and magnetic responses.

### 2.11. Toxicity study

In vitro toxicity testing of the liposomes, the MLs and the PpIX-loaded MLs was performed using MCF-7 cells, which were obtained from Adnan Menderes University, Science Technology Research and Application Center, Aydin, Turkey. The cells were given DMEM supplemented with 10% fetal bovine serum and 1 mM sodium pyruvate and maintained at 37 °C in a $CO_2$ incubator containing 5% $CO_2$. The cells were seeded at a density of 10,000 cells per well in a flat bottom 96-well plate, and media was refreshed after 24 h. The PpIX-loaded MLs were diluted in complete media at different concentrations of PpIX, ranging from 25 nM to 350 nM, and added in wells. The same volume of MLs and liposomes were prepared at a variety of concentrations considering the volume of PpIX-loaded MLs added to the wells. After the addition of the liposomes, the MLs and the PpIX-loaded MLs into the wells, the cells were incubated again for 24 and 48 h. Then, cell viability was assessed using an MTT assay kit (Roche, Germany).

### 2.12. In vitro PDT study

MCF-7 cell culture and preparation of liposomes, MLs and PpIX-loaded MLs is described above. After adding the samples to the cells, the cells were incubated for 3 h and subsequently exposed to white diode light for 1, 3 and 5 min from a 3-cm height. Free PpIX dissolved in 0.5% DMSO was irradiated for 5 min. The LED downlight (20 W) was purchased from Epistar, Taiwan; the LED was 3000 K white, 17 cm in application diameter and emitted 1650 lumens. The LED downlight was chosen because PpIX exhibits maximum absorbance at 409 nm light but also absorbs components at longer wavelengths in the visible light range [21], and white light contains all visible light, ranging from 400 to 700 nm. Furthermore, when considering the LED downlight properties and size, the heat generated by the light is very low and it is useful for the exposure of an entire 96-well plate. The cells were incubated again for 24 h after sample addition; in other words, the cells were incubated for 21 h after white light exposure. Subsequently, cell viability was determined by the MTT assay.

## 3. Results

### 3.1. Characterization and optimization of PpIX-loaded MLs

The PpIX-loaded MLs appeared brown because of both the PpIX and the $Fe_3O_4$ nanoparticles. Increasing or decreasing the amount of either the PpIX or the $Fe_3O_4$ nanoparticles affected the color of the suspension, but the nanoparticles were inherently dominated the determination of sample color. The UV absorption spectrum of free PpIX, $Fe_3O_4$ nanoparticles and PpIX-loaded MLs are shown in Fig. 1. Concentration and lipid amount were constant for the entire experiment. To investigate $Fe_3O_4$ nanoparticle efficacy, different amounts of $Fe_3O_4$ nanoparticles (0.175, 0.35 and 0.5 mg) were studied, while 20 μM PpIX was kept constant in PpIX-loaded ML preparation. As shown in Table 1, the PpIX-loaded ML average hydrodynamic diameter, polydispersity index (PDI) and zeta potential depended on the number of nanoparticles.

High zeta potential (negative or positive) prevents magnetoliposome aggregation; therefore, 0.5 mg $Fe_3O_4$ nanoparticles was selected for further study. To investigate the effect of PpIX on size and zeta potential, a variety of PpIX concentrations (20, 40 and 60 μM) were used to prepare the PpIX-loaded MLs while keeping the amount of $Fe_3O_4$ nanoparticles constant at 0.5 mg. Average size, PDI and zeta potential changes are shown in Table 2.

TEM analyses were performed without staining the samples. The ML sizes were smaller than 200 nm, whereas PpIX-loaded ML size varied between 166 and 720 nm (Fig. 2). TEM images show the color of the PpIX-loaded MLs to be darker compared to the MLs, and when the PpIX-loaded MLs were 200 nm or smaller, they were quite dark and perfectly spherical (Fig. 2D).

### 3.2. Iron content of PpIX-loaded MLs

The calculated non-dialyzed PpIX-loaded ML Fe content was approximately 1.7 times higher than the Fe content measured

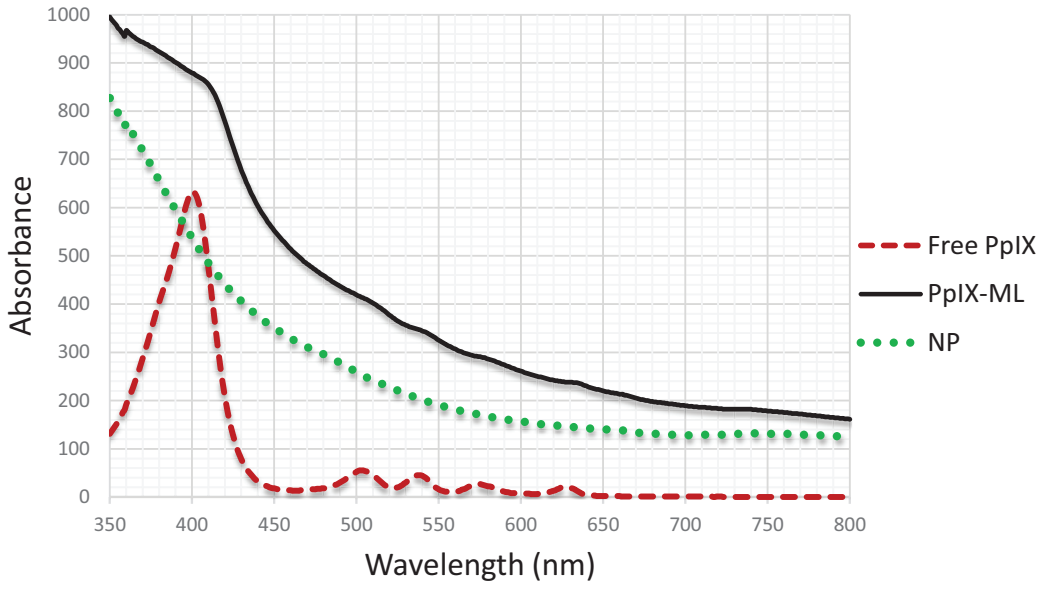


**Fig. 1.** UV absorption spectra of PpIX (dissolved in 0.5% DMSO in PBS), $Fe_3O_4$ nanoparticles in water and PpIX-loaded MLs (PpIX-ML) in water. The ascent of PpIX-ML between 450 and 409 nm was caused by PpIX.

**Table 1**
Hydrodynamic diameter (size), polydispersity index (PDI) and zeta potential of dialyzed and non-dialyzed PpIX-loaded MLs. The values are shown as the mean ± standarddeviation for each group ($n = 3$). Concentration of PpIX was constant as 20 μM and different amounts of $Fe_3O_4$ nanoparticles (0.175, 0.35 and 0.5 mg) were used to produce the PpIX-loaded MLs.

| Name of sample | Size (nm) mean [R:max–min] | (PDI) mean ± stddev | Zeta potential (mV) mean ± stddev |
|---|---|---|---|
| ML-$PpIX_{(20)}$-(0.175 mg $Fe_3O_4$) | 169.1 [3.4] | (0.164 ± 0.008) | −5.3 ± 1.1 |
| ML-$PpIX_{(20)}$-(0.175 mg $Fe_3O_4$)-Dialyzed | 178.4 [2.7] | (0.178 ± 0.008) | −8.1 ± 0.6 |
| ML-$PpIX_{(20)}$-(0.35 mg $Fe_3O_4$) | 174.5 [9.5] | (0.188 ± 0.017) | −10.4 ± 0.8 |
| ML-$PpIX_{(20)}$-(0.35 mg $Fe_3O_4$)-dialyzed | 207.8 [6.3] | (0.323 ± 0.047) | −9.53 ± 0.4 |
| ML-$PpIX_{(20)}$-(0.5 mg $Fe_3O_4$) | 166.0 [4.0] | (0.155 ± 0.019) | −11.1 ± 0.2 |
| ML-$PpIX_{(20)}$-(0.5 mg $Fe_3O_4$)-dialyzed | 211.0 [18.4] | (0.380 ± 0.023) | −10.8 ± 1.2 |

**Table 2**
Size, PDI and zeta potential of dialyzed and non-dialyzed PpIX-loaded MLs. The values are shown as the mean ± standarddeviation for each group ($n = 3$). PpIX-loaded MLs were synthesized with 0.5 mg $Fe_3O_4$ nanoparticles for each group. Different concentrations of PpIX (20, 40 and 60 μM) were used to produce the PpIX-loaded MLs.

| Name of sample | Size (nm) mean [R:max–min] | (PDI) mean ± stddev | Zeta potential (mV) mean ± stddev |
|---|---|---|---|
| ML-$PpIX_{(20)}$ | 166.0 [4.0] | (0.155 ± 0.019) | −11.1 ± 0.2 |
| ML-$PpIX_{(20)}$-dialyzed | 211.0 [18.4] | (0.380 ± 0.023) | −10.8 ± 1.2 |
| ML-$PpIX_{(40)}$ | 166.1 [9.8] | (0.130 ± 0.025) | −11.9 ± 1.3 |
| ML-$PpIX_{(40)}$-dialyzed | 221.8 [1.6] | (0.331 ± 0.040) | −10.8 ± 0.9 |
| ML-$PpIX_{(60)}$ | 164.2 [2.9] | (0.200 ± 0.011) | −9.28 ± 0.5 |
| ML-$PpIX_{(60)}$-dialyzed | 230.6 [28.9] | (0.394 ± 0.019) | −7.78 ± 0.3 |

by ICP-MS, and linear increments existed in both the calculated and the measured values. The percentage of encapsulated $Fe_3O_4$ nanoparticles in dialyzed samples was 83.96% for the 0.175 mg initial nanoparticle addition, 91.67% for the 0.35 mg initial nanoparticle addition and 80.85% for the 0.5 mg initial nanoparticle addition; these were calculated by comparing the percentage of Fe content between dialyzed and non-dialyzed samples.

### 3.3. Encapsulation efficiency

Dialyzed and non-dialyzed PpIX-loaded MLs were used to calculate the percentage of PpIX encapsulation depending on fluorescence emission; therefore, the percentage of encapsulation is also the encapsulation efficiency of dialyzed samples, which is shown in Fig. 3A. The mean values of PpIX encapsulation percentage for 20 μM and 40 μM PpIX-loaded MLs were similar; they were 65.55 ± 2.09 and 67.65 ± 1.93, respectively. In contrast, the PpIX encapsulation percentage of 60 μM PpIX-loaded MLs was calculated as 81.65 ± 1.05.

The PpIX encapsulation percentages were multiplied by the initial concentrations of PpIX, which were used for fabricating the PpIX-loaded MLs, to obtain the concentration of encapsulated PpIX (Fig. 3B). Although percent fluorescence intensities similar for $PpIX_{(20)}$ and $PpIX_{(40)}$, $PpIX_{(40)}$ concentration was almost twice that of $PpIX_{(20)}$ because dialyzed and non-dialyzed PpIX-loaded MLs were used to calculate the concentrations. Considering all these results (size, zeta potential, fluorescence emission etc.) and the volume of PpIX-loaded MLs to be applied to cell culture, $PpIX_{(40)}$ was chosen for further experiment.

### 3.4. Temperature effects

The percentage of PpIX release at different temperatures (37 °C and 42 °C) within 1 hour indicated that PpIX release at 42 °C at any time was lower than that of 37 °C, which was not rational

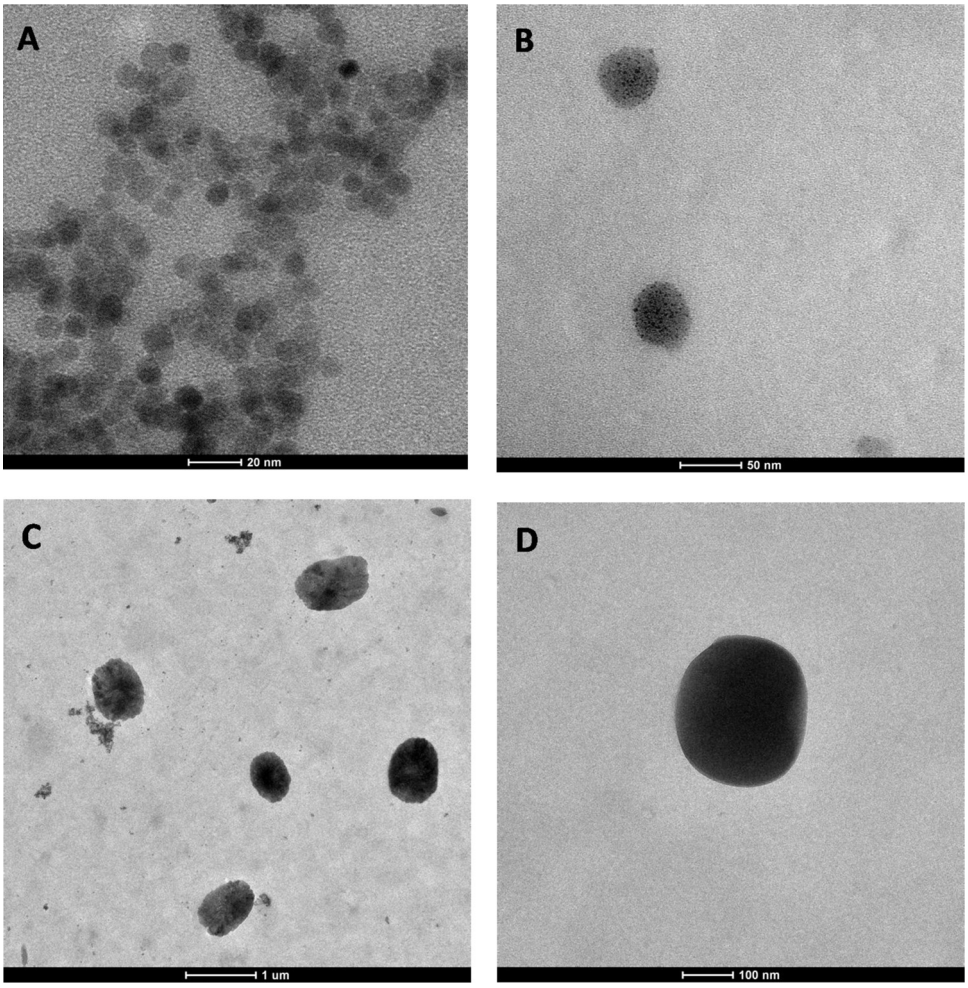


**Fig. 2.** TEM images of nanoparticles, MLs and PpIX-loaded MLs. (A) $Fe_3O_4$ nanoparticles with a homogenous size distribution with 10 nm diameters. (B) MLs that are smaller than 200 nm; black dots in MLs are nanoparticles. (C) PpIX-loaded MLs with different sizes. (D) Spherically shaped PpIX-loaded MLs that are approximately 200 nm in size.

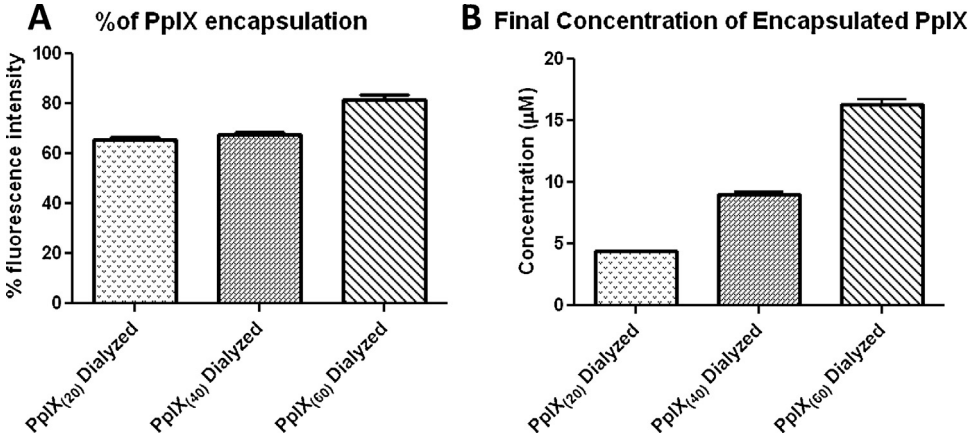


**Fig. 3.** (A) Percentage of PpIX encapsulation of dialyzed PpIX-loaded MLs depending on fluorescence intensity ($n = 3$). There is no significant difference between $PpIX_{(40)}$ and $PpIX_{(20)}$, but there is a significant difference $PpIX_{(60)}$ and the other groups ($p < 0.05$). (B) Final concentration of PpIX after dialysis. There are significant differences among each group ($p < 0.05$).

(Supplementary material Fig. 1A). It should not be related to the release of PpIX, but to the aggregation of highly released PpIX. Fluorescence intensity percentages indicated fluorescence emission of PpIX for different temperatures (Supplementary material Fig. 1B and C).

### *3.5. Temperature changes of PpIX-loaded MLs under an electromagnetic field*

Temperature changes were observed for both water and PpIX-loaded MLs under AC magnetic field. Effect of PpIX-loaded MLs on temperature changes were obtained by subtracting the tempera-

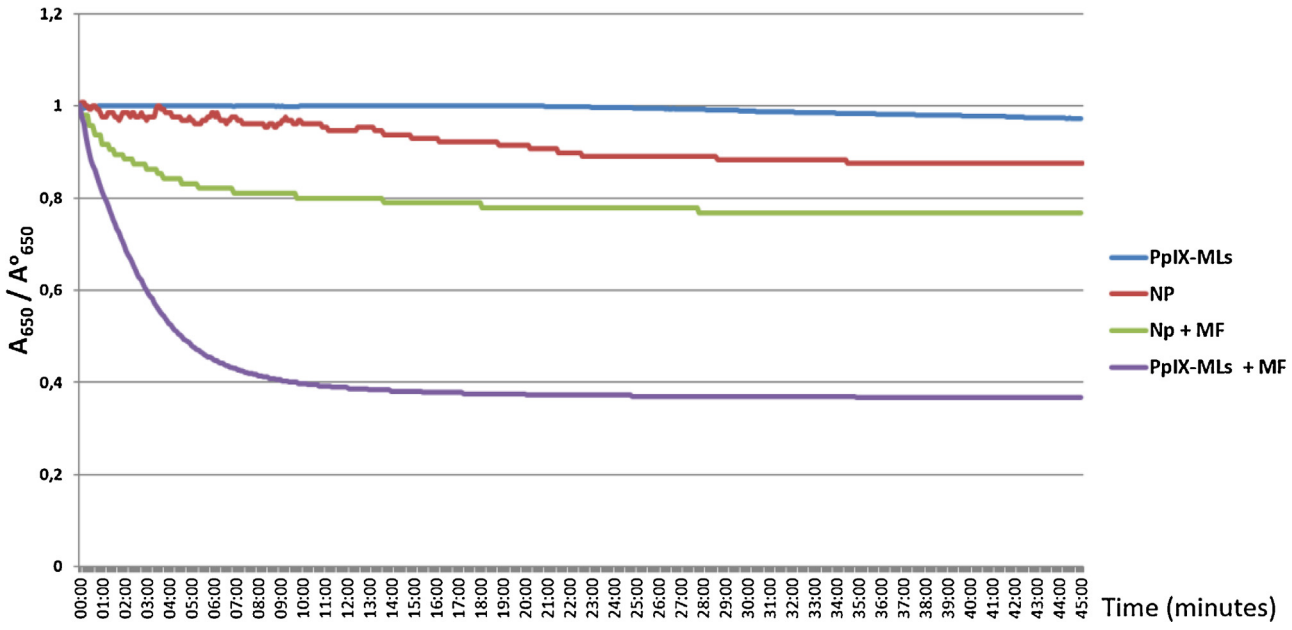


**Fig. 4.** Spectrophotometric analysis of magnetic response of PpIX-loaded MLs (PpIX-MLs) and $Fe_3O_4$ nanoparticles (NP) under a permanent magnetic field (MF).

ture of the water from the temperature of the PpIX-loaded MLs. Temperature of the PpIX-loaded MLs increased by 0.9 °C within 30 min and by 1.5 °C within 60 min under an 8.947 ± 2% μT AC electromagnetic field.

### 3.6. Turbidity assessment

There was almost no sedimentation observed during turbidity measurements for the PpIX-loaded MLs, but almost 10% sedimentation was observed for the $Fe_3O_4$ nanoparticles within 45 min. However, under the effect of permanent magnets, small amounts of nanoparticles accumulated on the cuvette walls where the magnets were positioned. Cuvette wall accumulation was highest for the PpIX-loaded MLs, leading to decreased absorbance $A_{650}/A°_{650}$ rates (Fig. 4).

### 3.7. Toxicity analysis

Viability of cells that did not receive light exposure (dark toxicity) was evaluated using the MTT assay. Percentages of viable cells after 24 h and 48 h were shown in Fig. 5A and B. Average viability of cells that received the highest PpIX-ML concentrations ($V_{350}$) were 66% after 24 h and 55% after 48 h.

### 3.8. In vitro PDT results

Cell viability after receiving liposomes and ML groups with 1, 3 and 5 min of irradiation was similar to viability of cells incubated for 24 h without having received light exposure. In the PpIX-loaded ML group, cell viability decreased with increasing irradiation time (Fig. 6). After 5 min of irradiation, cell viabilities were determined to be 0% for PpIX-ML concentrations of 250 nM and higher and slightly higher for free PpIX, but the difference was not significance ($p > 0.05$) because of the high standard error of the free PpIX data. Slightly higher cell viability with the free PpIX may have been caused by the relatively low stimulation of aggregated PpIX molecules. Although PpIX dissolves in 100% DMSO, absorbance rate decreases when the ratio of DMSO in PBS decreases (Fig. 7), which may be the result of aggregation. Only 350 nM PpIX concentrations caused 0% cell viability after 3 min of irradiation. Experiments with longer periods of light irradiation were also performed. When the light exposure time exceeded 10 min, the cells containing concentrations of PpIX in MLs of 150 nM and higher, cell viability was found to be 0% (data not shown).

## 4. Discussion

Liposomes have been frequently used as targeted drug delivery agents. Liposomes or particles must be smaller than 5 μm to be delivered in the bloodstream because the smallest capillaries in the body have a 5–6 μm radius, and the use of larger liposomes or particles may result in embolism [16]. $PpIX_{(40)}$-loaded MLs (dialyzed) were 221.8 ± 0.8 nm in size with a 0.331 PDI dynamic light scattering (DLS) measurement, which indicated that the samples had a good quality size distribution and were small enough for intravenous administration. However, TEM images showed that the sizes of the $PpIX_{(40)}$-loaded MLs (dialyzed) were between 166 and 720 nm. We think that some of the closely aggregated PpIX molecules may have gathered lipids around the aggregate surfaces, leading to larger or multi-lamellar PpIX-loaded MLs. PpIX may be responsible for aggregation-dependent size increments because the MLs were smaller than 200 nm, and the only difference between the MLs and the PpIX-loaded MLs was PpIX. However, one possible reason for observing larger sizes of PpIX-loaded MLs is that this may be an effect of the drying process on the TEM grid. PpIX is a hydrophobic molecule; hence, it most likely formed lipid bilayers, and the $Fe_3O_4$ nanoparticles were likely located in the center of the vesicles. The nanoparticles demonstrated hydrophilic properties because they were observed to be stable in water. When the PpIX-loaded MLs were 200 nm or smaller, the vesicles were almost perfectly spherical, which suggested that 200 nm was a critical diameter for obtaining a spherical shape. However, cryo-TEM analysis would be more helpful in determining the relative locations of the PpIX and the nanoparticles in the lipid bilayers as well as the factors affecting PpIX-loaded ML size and shape.

Concerning the encapsulation of the iron oxide nanoparticles in the PpIX-loaded MLs, the highest rate of Fe content was observed to be 91.67% for the dialyzed sample with the initial addition of 0.35 mg $Fe_3O_4$ nanoparticles. However, the highest amount of encapsulated nanoparticles was obtained by the sample that

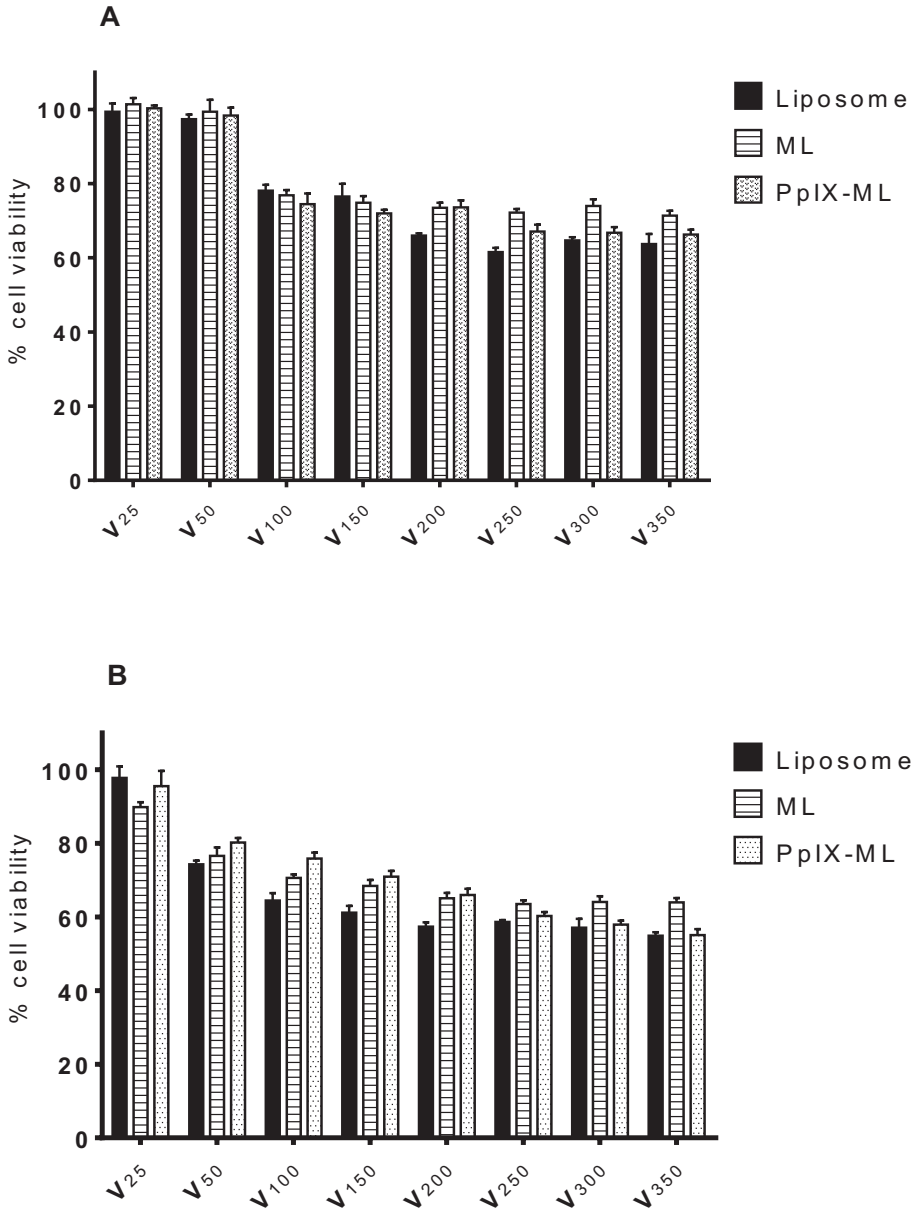


**Fig. 5.** Cytotoxic effect of PpIX-loaded MLs (PpIX-ML), magnetoliposomes (ML) and liposomes on MCF-7 cells (mean ± SE, $n = 7$). (A) Cells incubated for 24 h. (B) Cells incubated for 48 h. Numbers near the letter **V** (25, 50, 100, etc.) indicate nanomolar concentrations of PpIX applied to cells via PpIX-ML, and the letter **V** indicates the volume of liposome and ML with the same volume of PpIX-ML applied to cells.

received the highest initial amount of nanoparticles, 0.5 mg $Fe_3O_4$ nanoparticles (80.85% Fe content). Frascione et al. [25]. reported a highest encapsulation efficiency of 92% for a sample that received MLs with an initial Fe concentration of 0.5 mg/ml, which were produced for magnetic resonance imaging.

The percentage of PpIX encapsulation was almost the same for $PpIX_{(20)}$ and $PpIX_{(40)}$, whereas $PpIX_{(60)}$ had approximately 14% higher PpIX encapsulation in comparison with the other PpIX-loaded ML groups; this may have resulted from fluorescence emission of unencapsulated but aggregated PpIX. Although $PpIX_{(40)}$ had two times more initial PpIX than $PpIX_{(20)}$, similar percentages of encapsulation efficiency were observed.

Temperature dependent percentage of PpIX release cannot be calculated by the%release formula as reported by Pradhan et al. [3]. for this experiment because released PpIX molecules aggregate in neutral water. As a result of this aggregation, only the outer surface of aggregated molecules might be stimulated by light and fluoresce. Therefore, fluorescence intensities of PpIX at 42 °C were observed to be smaller or slightly higher than fluorescence intensities at $t = 0$, which is not possible because the transition temperature of lipids is lower than 42 °C.

Percentage of fluorescence intensity for dialyzed PpIX-loaded MLs in decreasing order were $PpIX_{(20)} > PpIX_{(40)} > PpIX_{(60)}$. However, this result was not directly proportional to the amount of encapsulated PpIX, but was also influenced by the release rate of PpIX from the MLs and PpIX aggregation behavior. This result indicates that when PpIX molecules release rapidly, aggregation occurs. Therefore, we suggest that relatively slow release of PpIX at body temperature is more favorable.

Temperature changes of PpIX-loaded MLs under a low frequency AC magnetic field revealed that when the PpIX-loaded MLs were administered at body temperature, 50 Hz electromagnetic fields only caused a 1 °C change within 30 min. However, Kulshrestha et al. [26]. reported that temperature of paclitaxel-loaded MLs rose

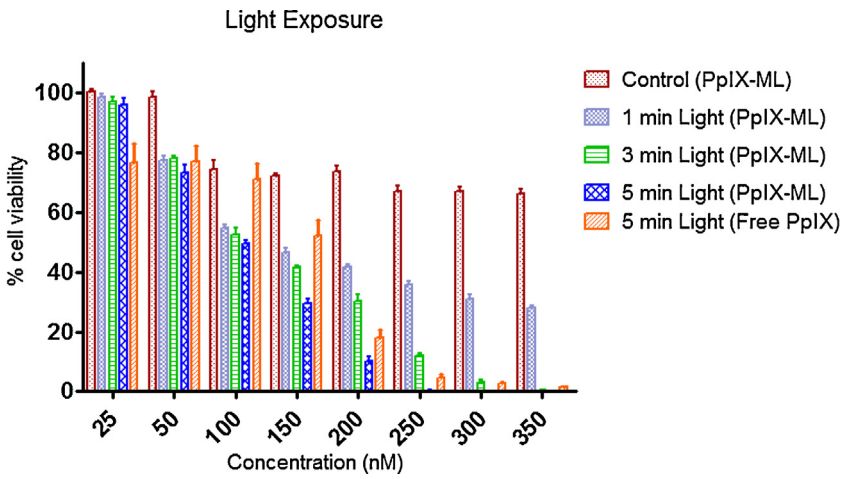


**Fig. 6.** Cell viability of MCF-7 cells exposed to various concentrations of PpIX-loaded MLs (PpIX-ML) and free PpIX after exposure to white light for 1, 3 and 5 min. Cell viability was assessed after 24 h of incubation. Control group was not exposed to white light (dark toxicity). Data are shown as the mean ± SEM ($n = 7$).

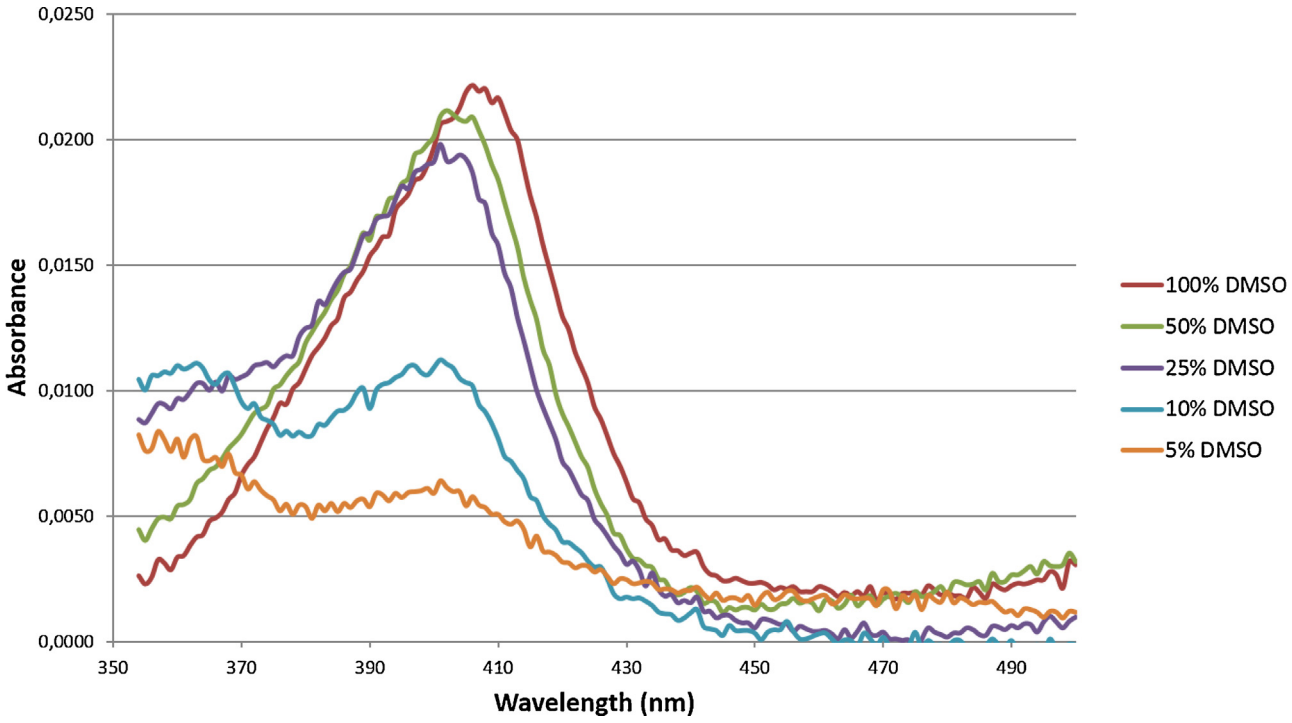


**Fig. 7.** Absorbance at 250 nM of PpIX in different ratios of DMSO:PBS.

from 25 °C to 43 °C within 30 min using a magnetic field with a 10-kA current and a 423-kHz frequency. Another report, published by Pradhan et al. [3], demonstrated that the temperature of folate-targeted MLs reached 42.5 °C within 15 min under a magnetic field with a 12-kA current and 290-kHz frequency. According to these results, high frequency and high current are needed to increase the temperature of MLs in a short time.

The purpose of the magnetic response assessment was to understand whether the vehicle is suitable for targeted, magnetic drug delivery applications. Magnetic response of the PpIX-loaded MLs was dependent on the magnetic properties and number of encapsulated magnetic nanoparticles. Although the PpIX-loaded MLs exhibited a 63% magnetic field response within 45 min, the response was not sufficient for magnetic targeting; as suggested by Vlaskou et al. [24], response needs to be 90% or higher. However, the response of the PpIX-loaded MLs to the magnetic field was higher than that of the nanoparticles, which exhibited approximately a 25% response to the magnetic field. It should also be noted that the PpIX-loaded MLs demonstrated no sedimentation within 45 min, which may be the result of their zeta potentials.

In view of the cytotoxic effects exerted by the liposomes, the MLs and the PpIX-loaded MLs at the highest concentrations, cell viability for all groups was observed to be higher than 63% after 24 h of incubation and higher than 55% after 48 h of incubation. The toxic effect of the liposomes was observed to be slightly higher than that of the MLs and the PpIX-loaded MLs after both 24 and 48 h of incubation. Soenen et al. [27]. reported similar results for 3T3 fibroblasts and explained that the slight protective effect was due to stable ML formation. These results suggested to us that lipid formation affects cell viability more than the number of nanoparticles used in this study, and it is likely that the stable nanoparticle-lipid formation

was responsible for this slightly lower toxicity. The reduction of cell viability could be due to the reactive oxygen species.

In previous studies, ALA-induced PpIX in cell culture was used with a range of ALA concentrations, which varied between 20 μM and 1 mM [28,29]. The concentration of PpIX that we used was at the nM level, and results indicate that direct usage of PpIX via MLs can yield effective results at very low concentrations (approximately 60 fold smaller than the ALA concentration).

Red lasers are usually used in PDT studies because tissue penetration of red is higher than the smaller wavelengths of visible light [30]. However, the absorbance wavelength of photosensitizers has to be considered to use them effectively for PDT. PpIX indicates maximum absorbance with approximately 400-nm light. It has been reported that the application of a 20-μM hexenyl ester of ALA and a 5-J/cm$^2$ red LED resulted in an approximately 80% MCF-7 cells survival rate after 24 h of incubation [28]. Fratz et al. [31]. have used ALA-induced PpIX in a variety of cell lines, and they used red light ($630 \pm 20$ nm) to measure toxicity. They found that toxicity changes depending on cell type (80% to 30%). We think that application of 400-nm light would result in higher toxicity for PDT using mediated ALA-induced PpIX. Therefore, we used white light, which contains light between 400 nm and 780 nm. Similarly, Tachikawa et al. [32]. produced PpIX-lipid micelles and applied these to Hela cells. The Hela cells were irradiated with a xenon lamp in the 400–800 nm wavelength range, and they also obtained toxicity using nM levels of PpIX. Additionally, Temizel et al. [33]. used 375 nm light to irradiate liposomal porphyrin. Therefore, according to all these reports, PpIX requires approximately 400-nm light to yield maximum efficiency. However, deep tissue efficacies of PpIX with white light in cancer therapy should be examined closely.

In our study, significant reduction in cell viability was observed depending on the amount of irradiation time received by the MCF-7 cells. When the light exposure had exceeded 10 min, all the cells exposed to 150 nM and higher concentrations of PpIX died, which should be the result of singlet oxygen production and/or other ROS. These in vitro results represent that the PpIX-loaded MLs that we produced are highly effective for PDT and that they enable the use of inexpensive, harmless white light instead of relatively expensive, high-energy lasers.

## 5. Conclusion

In the present study, we prepared PpIX-loaded MLs and studied their drug release behavior, toxicity and photodynamic effects. The results of the current study revealed that PpIX-loaded MLs produced are small enough for intravenous application and that aggregation behavior can be eliminated by regulating zeta potentials. When nano-molar concentrations of PpIX-loaded MLs were irradiated by LED white light, 100% cell death was caused in the MCF-7 cell line, which is one of the aggressive breast cancer cell lines. As a result, this study demonstrates that PpIX-loaded MLs are highly effective and promising structures for PDT. Furthermore, the PpIX-loaded ML has potential to be used in magnetic resonance imaging because of the iron oxide nanoparticle content and is also a suitable structure for targeted therapy. However, future in vivo studies should be carried out to determine the behavior of the PpIX-loaded MLs in physiological environments.

## Acknowledgements

Support from the Scientific and Research Council of Turkey (TUBITAK) (grant no: 112S958) and Adnan Menderes University, Aydın Turkey (grant no: TPF-13014) is gratefully acknowledged. The authors thank the Izmir Institute of Technology, Biotechnology and Bioengineering Research and Application Center, and Adnan Menderes University, Science Technology Research and Application Center for providing laboratory facilities and equipment.

## Appendix A. Supplementary data

Supplementary data associated with this article can be found, in the online version, at http://dx.doi.org/10.1016/j.pdpdt.2015.12.010.

## References

[1] D. Qiu, X. An, Z. Chen, X. Ma, Microstructure study of liposomes decorated by hydrophobic magnetic nanoparticles, Chem. Phys. Lipids 165 (2012) 563–570.
[2] H.R. Samadikhah, A. Majidi, M. Nikkhah, S. Hosseinkhani, Preparation, characterization, and efficient transfection of cationic liposomes and nanomagnetic cationic liposomes, Int. J. Nanomed. 6 (2011) 2275–2283.
[3] P. Pradhan, J. Giri, F. Rieken, C. Koch, O. Mykhaylyk, M. Doblinger, et al., Targeted temperature sensitive magnetic liposomes for thermo-chemotherapy, J. Controll. Release 142 (2010) 108–121.
[4] G.D. Bothun, A. Lelis, Y. Chen, K. Scully, L.E. Anderson, M.A. Stoner, Multicomponent folate-targeted magnetoliposomes: design, characterization, and cellular uptake, Nanomed. Nanotechnol. Biol. Med. 7 (2011) 797–805.
[5] B. Garnier, S. Tan, S. Miraux, E. Bled, A.R. Brisson, Optimized synthesis of 100 nm diameter magnetoliposomes with high content of maghemite particles and high MRI effect, Contrast Media Mol. Imaging 7 (2012) 231–239.
[6] M.R. Faria, M.M. Cruz, M.C. Goncalves, A. Carvalho, G. Feio, M.B. Martins, Synthesis and characterization of magnetoliposomes for MRI contrast enhancement, Int. J. Pharm. 446 (2013) 183–190.
[7] M. De Cuyper, S.J. Soenen, K. Coenegrachts, L.T. Beek, Surface functionalization of magnetoliposomes in view of improving iron oxide-based magnetic resonance imaging contrast agents: anchoring of gadolinium ions to a lipophilic chelate, Anal. Biochem. 367 (2007) 266–273.
[8] S.J. Soenen, M. De Cuyper, How to assess cytotoxicity of (iron oxide-based) nanoparticles: a technical note using cationic magnetoliposomes, Contrast Media Mol. Imaging 6 (2011) 153–164.
[9] M.D. Bilgin, A.E. Elcin, Y.M. Elcin, Topical use of liposomal copper palmitate formulation blocks porphyrin-induced photosensitivity in rats, J. Photochem. Photobiol. B 80 (2005) 107–114.
[10] R. Ackroyd, C. Kelty, N. Brown, M. Reed, The history of photodetection and photodynamic therapy, Photochem. Photobiol. 74 (2001) 656–669.
[11] D.K. Chatterjee, L.S. Fong, Y. Zhang, Nanoparticles in photodynamic therapy: an emerging paradigm, Adv. Drug Deliv. Rev. 60 (2008) 1627–1637.
[12] W.M. Sharman, C.M. Allen, J.E. van Lier, Photodynamic therapeutics: basic principles and clinical applications, Drug Discov. Today 4 (1999) 507–517.
[13] A.E. O'Connor, W.M. Gallagher, A.T. Byrne, Porphyrin and nonporphyrin photosensitizers in oncology: preclinical and clinical advances in photodynamic therapy, Photochem. Photobiol. 85 (2009) 1053–1074.
[14] D.E. Dolmans, A. Kadambi, J.S. Hill, K.R. Flores, J.N. Gerber, J.P. Walker, et al., Targeting tumor vasculature and cancer cells in orthotopic breast tumor by fractionated photosensitizer dosing photodynamic therapy, Cancer Res. 62 (2002) 4289–4294.
[15] M. Fadel, K. Kassab, D.A. Fadeel, Zinc phthalocyanine-loaded PLGA biodegradable nanoparticles for photodynamic therapy in tumor-bearing mice, Lasers Med. Sci. 25 (2010) 283–292.
[16] E. Ricci-Junior, J.M. Marchetti, Zinc(II) phthalocyanine loaded PLGA nanoparticles for photodynamic therapy use, Int. J. Pharm. 310 (2006) 187–195.
[17] D. Fayter, M. Corbett, M. Heirs, D. Fox, A. Eastwood, A systematic review of photodynamic therapy in the treatment of pre-cancerous skin conditions, Barrett's oesophagus and cancers of the biliary tract, brain, head and neck, lung, oesophagus and skin, in: NIHR Health Technology Assessment programme: Executive Summaries, NIHR Evaluation, Trials and Studies Coordinating Centre (UK), Southampton (UK), 2010, pp. 1–129.
[18] E. Cabuy, Photodynamic therapy in cancer treatment, Reliable cancer therapies, Energy Based Ther. (2012) 1–54.
[19] I. Inamura, K. Uchida, Association behavior of protoporphyrin IX in water and aqueous poly(*N*-vinylpyrrolidone) solutions. Interaction between protoporphyrin IX and poly(*N*-vinylpyrrolidone), Bull. Chem. Soc. Jpn. 64 (1991) 2005–2007.
[20] Q. Liu, X. Wang, P. Wang, H. Qi, K. Zhang, L. Xiao, Sonodynamic effects of protoporphyrin IX disodium salt on isolated sarcoma 180 cells, Ultrasonics 45 (2006) 56–60.
[21] L.M. Scolaro, M. Castriciano, A. Romeo, S. Patane, E. Cefali, M. Allegrini, Aggregation behavior of protoporphyrin IX in aqueous solutions: clear evidence of vesicle formation, J. Phys. Chem. B. 106 (10) (2002) 2453–2459.
[22] L. Gandara, E. Sandes, G. Di Venosa, B. Prack Mc Cormick, L. Rodriguez, L. Mamone, et al., The natural flavonoid silybin improves the response to photodynamic therapy of bladder cancer cells, J. Photochem. Photobiol. B 133 (2014) 55–64.
[23] Z. Mohammadi, A. Sazgarnia, O. Rajabi, S. Soudmand, H. Esmaily, H.R. Sadeghi, An in vitro study on the photosensitivity of 5-aminolevulinic acid conjugated gold nanoparticles, Photodiagn. Photodyn. Ther. 10 (2013) 382–388.

[24] D. Vlaskou, O. Mykhaylyk, F. Krötz, N. Hellwig, R. Renner, U. Schillinger, et al., Magnetic and acoustically active lipospheres for magnetically targeted nucleic acid delivery, Adv. Funct. Mater. 20 (2010) 3881–3894.
[25] D. Frascione, C. Diwoky, G. Almer, P. Opriessnig, C. Vonach, K. Gradauer, et al., Ultrasmall superparamagnetic iron oxide (USPIO)-based liposomes as magnetic resonance imaging probes, Int. J. Nanomed. 7 (2012) 2349–2359.
[26] P. Kulshrestha, M. Gogoi, D. Bahadur, R. Banerjee, In vitro application of paclitaxel loaded magnetoliposomes for combined chemotherapy and hyperthermia, Colloids Surf. B: Biointerfaces 96 (2012) 1–7.
[27] S.J. Soenen, A.R. Brisson, M. De Cuyper, Addressing the problem of cationic lipid-mediated toxicity: the magnetoliposome model, Biomaterials 30 (2009) 3691–3701.
[28] J.H. Yoon, H.E. Yoon, O. Kim, S.K. Kim, S.G. Ahn, K.W. Kang, The enhanced anti-cancer effect of hexenyl ester of 5-aminolaevulinic acid photodynamic therapy in adriamycin-resistant compared to non-resistant breast cancer cells, Lasers Surg. Med. 44 (2012) 76–86.
[29] S. Sharma, A. Jajoo, A. Dube, 5-Aminolevulinic acid-induced protoporphyrin-IX accumulation and associated phototoxicity in macrophages and oral cancer cell lines, J. Photochem. Photobio. B: Biol. 88 (2007) 156–162.
[30] A.M. Smith, M.C. Mancini, S. Nie, Bioimaging second window for in vivo imaging, Nat. Nanotechnol. 4 (2009) 710–711.
[31] E.J. Fratz, G.A. Hunter, G.C. Ferreira, Expression of murine 5-aminolevulinate synthase variants causes protoporphyrin IX accumulation and light-induced mammalian cell death, PLoS one 9 (2014) e93078.
[32] S. Tachikawa, M.E. El-Zaria, R. Inomata, S. Sato, H. Nakamura, Synthesis of protoporphyrin-lipids and biological evaluation of micelles and liposomes, Bioorg. Med. Chem. 22 (2014) 4745–4751.
[33] E. Temizel, T. Sagir, E. Ayan, S. Isik, R. Ozturk, Delivery of lipophilic porphyrin by liposome vehicles: preparation and photodynamic therapy activity against cancer cell lines, Photodiagn. Photodyn. Ther. 11 (2014) 537–545.